Materials and Design 194 (2020) 108901

Contents lists available at ScienceDirect

Materials and Design

journal homepage: www.elsevier.com/locate/matdes

Superior mechanical and optical properties of a heterogeneous library of cross-linked biomimetic self-assembling peptides

Raffaele Pugliese [a], Luca Moretti [b], Margherita Maiuri [b], Tiziana Romanazzi [c,d], Giulio Cerullo [b], Fabrizio Gelain [a,c,*]

[a] Tissue Engineering Unit, Institute for Stem Cell Biology, Regenerative Medicine and Innovative Therapies-ISBReMIT, Fondazione IRCCS Casa Sollievo della Sofferenza, San Giovanni Rotondo, FG, Italy
[b] IFN_CNR, Dipartimento di Fisica, Politecnico di Milano, Milan, Italy
[c] Center for Nanomedicine and Tissue Engineering (CNTE), ASST Grande Ospedale Metropolitano Niguarda, Milan, Italy
[d] Bioscience, Biotechnology and Bioinformatics Department, University of Bari "Aldo Moro", Bari, Italy

HIGHLIGHTS

- Genipin increases mechanical properties of various lysine-containing SAPs while maintaining their nanofibrous structure.
- Cross-linking reaction does not involve the bioactive motifs, thus preserving the SAP biomimetic properties.
- Cross-linking boosts SAP thermostability beyond 100°C.
- Cross-linking reaction allows for charge transfer between cross-linked peptide chains.
- Optical properties of cross-linked SAPs are changed showing absorption and fluorescence bands in the visible spectral range.

GRAPHICAL ABSTRACT

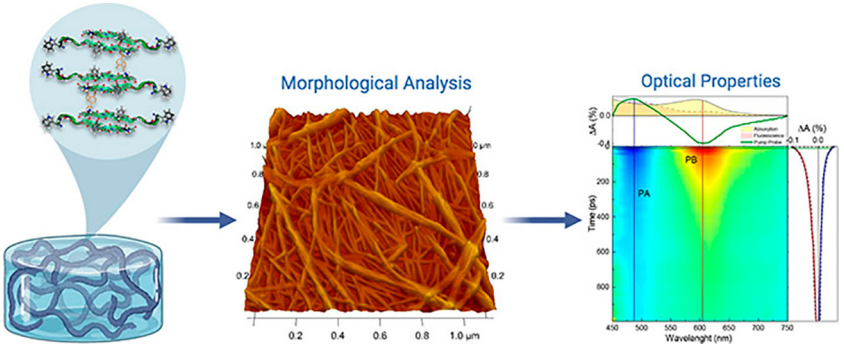

ARTICLE INFO

Article history:
Received 22 April 2020
Received in revised form 13 June 2020
Accepted 18 June 2020
Available online 25 June 2020

Keywords:
Self-assembling peptides
Cross-linking
Genipin
Mechanical properties
Pump-probe spectroscopy
Charge transfer

ABSTRACT

Self-assembling peptides (SAP) are ideal components for biomedical devices. However, their practical applications have been limited due to their intrinsic unstable, low-performance, and low-stress response given by non-covalent interactions involved in self-assembling. Herein, a library of SAPs featuring different self-assembled nanostructures was successfully cross-linked with genipin, allowing to produce nanofibrous hydrogels with enhanced mechanical properties ($G' \geq 0.2$ MPa, stress-failure ≥ 3.5 kPa) and enhanced thermostability (≥100 °C) while maintaining their native nanoarchitecture. Cross-linking dramatically changed the optical properties of SAPs: it triggered new absorption/fluorescence bands in the visible spectral range, which are attributed to charge transfer between peptide chains. Genipin cross-linking, fitted for different classes of SAPs, could be a powerful tool to obtain biomimetic SAP scaffolds with tunable stiffness and thermostability. Lastly, because of the changed absorption/emission properties and relaxation kinetics of cross-linked SAPs, genipin cross-linking may bestow novel optical properties to several well-known lysine-containing SAPs, with intriguing potential for biomedical imaging, photonics and optoelectronics.

* Corresponding author at: Center for Nanomedicine and Tissue Engineering (CNTE), ASST Grande Ospedale Metropolitano Niguarda, Milan, Italy.
E-mail address: f.gelain@css-mendel.it (F. Gelain).

https://doi.org/10.1016/j.matdes.2020.108901

1. Introduction

"About 10,000 years ago, humans began to domesticate plants and animals. Now it's time to domesticate molecules", said Susan Lindquist (Whitehead Institute for Biomedical Research - MIT). Indeed, scientists have designed new molecular patterns that can serve as a blueprint of new materials and sophisticate molecular machines [1]. In the field of nanotechnology, natural building blocks such as amino acids and/or oligopeptides are used to create molecular structures for applications in medicine [2], photonics [3], and electronics [4]. Two-decades ago, nanobiotechnologists have begun to exploit molecular self-assembly of peptides [5] to build nanostructured scaffolds aimed to repair damaged organs and tissues [6–11], or yielding nanovesicles for drug encapsulation [12–14] and nanocarriers for gene delivery [15].

Nature itself is the grandmaster when it comes to building high-performance materials: it is capable of precisely regulating not only the architecture (e.g. nanotopography) but also mechanical stiffness and error-correction capability (e.g. self-sustainability) of materials in space and time. For instance, actin, the major constituent of the cytoskeletal network of eukaryotic cells, is bundled with cross-linked filaments of actin-binding proteins, leading to porous and nanofibrous networks with unique mechanical properties: its stiffness can vary widely along with small changes in cross-links density, and can markedly increase upon application of external stimuli. These peculiar properties make the actin filaments essential in a variety of cellular processes, including motility, and mechanoprotection [16]. Other biological nanostructured gels, such as fibrin, the main structural protein in blood clots and acting as a scaffold to promote wound repair, show analogous architectures and properties. As a matter of fact, fibrin gels are among the most resilient gels in nature; they stiffen strongly when deformed and thereby become increasingly resistant to further deformation [17].

In stark contrast, synthetic self-assembling peptides (SAPs) nanofibrous gels, studied for many biomedical applications (e.g. hemostat solutions [11,18], bone fillers [19,20], wound healers [21,22], injectable scaffolds for the regeneration of injured heart [23] and spinal cord [6,24,25]) usually feature poor mechanical stability and are not stress-responsive. This is due to the transient weak non-covalent interactions involved in the self-assembling phenomenon; indeed, SAP assemblies interact through electrostatic attractions, H-bonds, van der Waal's forces, π-π stacking, and hydrophobic forces. Tuning of SAP biomechanics is usually achieved before triggering self-assembling by changing their concentration (when in solution), their self-assembling environment (e.g. temperature, solvents, or ionic strength), the density of bioactive functional motifs (if any) tethered to the self-assembling backbone: as such, altering the self-assembling kinetics, pore size and final conformation of entangled nanostructures [26–28]. Alternative strategies for tuning SAP biomechanics are the usage of chemical cross-linkers [29–32] or modifications of the ratio of oppositely charged co-assembling peptides [25,33]. Nonetheless, chemical cross-linking has to be carefully weighted in biological applications as unselective cross-linking of peptides and proteins found in cells and tissue may cause biocompatibility and toxicity issues.

Recently we introduced chemical cross-linking based on genipin, a naturally occurring cross-linking agent used in Chinese medicine [34–36] that specifically reacts with primary amines of peptides and proteins (Supplementary Scheme S1), as a reliable strategy to improve mechanical features (e.g. stiffness and stress-response) of FAQ$(LDLK)_3$, a self-assembling peptide hydrogel [30]. However, feasibility of genipin cross-linking reaction with other classes of SAPs, and opto-electronic properties as well as stability of genipin cross-linked SAPs were all missing pieces to the bigger picture.

Here, we demonstrate how the genipin cross-linking can be adopted with a number of different lysine-containing SAPs (pure, mixtures, linear, branched, biotinylated) to produce nanofibrous networks with increased mechanical properties and thermostability while maintaining their native nanoarchitecture. Similarly to the abovementioned actin and fibrin networks, we selectively cross-linked different SAP-molecules inside the assembled bundles, without altering their networks nanoarchitecture. Further, we also show how the efficiency of cross-linking (measured by stiffness and β-sheet packing increments) is primarily correlated with the total amount of β-structures present before the cross-linking reaction itself. We also show that the cross-linking reaction does not involve the residues of the bioactive functional motifs, usually not involved in backbone β-structuring, thus potentially preserving the biomimetic properties of cross-linked multi-functionalized SAPs. Lastly, we demonstrate that cross-linking deeply changes the optical properties of SAPs, giving rise to absorption and fluorescence bands in the visible spectral range, paving the way to novel optoelectronic and photonic applications of cross-linked SAPs.

This approach is potentially useful for any lysine-containing SAP and may be a precious tool to better tailor the biomechanics of nanostructured scaffolds/devices entirely made of SAPs, providing them with novel resilience, stress-stiffening, and optoelectronic properties to suit the needs of different applications in tissue engineering and beyond.

2. Methods

All reagents and solvents used for the peptide synthesis and characterizations were purchased from commercial sources and used without further purification. See Supplementary information for further experimental details.

2.1. General procedure for peptide synthesis and purification

All peptides were synthesized by solid-phase Fmoc-based chemistry on Rink amide 4-methyl-benzhydrylamine resin (0.5 mmol g^{-1} substitution) by using the Liberty-Discovery (CEM) microwave automated synthesizer. Peptides were subsequently purified via Waters binary HPLC apparatus, and the molecular weight of each peptide was identified via single quadrupole mass detection (Waters LC-MS Alliance-3100) (Supplementary Fig. S1).

2.2. Sample preparation

The peptides for structural, mechanical, and optical analyses were dissolved in distilled water (GIBCO®). After 24 h, 170 mM of genipin (Guangxi Shanyun Biochemical Science and Technology Co., Ltd.) solution was added to the samples for the cross-linking reaction, as previously described [30]. Briefly, genipin powder was dissolved in 100 μl of DPBS (Ca^{2+}/Mg^{2+} free) and EtOH (95:5 v/v; pH = 7.4), and filtered (0.22 μm pore size). Genipin cross-linked peptides were prepared by adding 170 mM of genipin to 50 μl of peptide (from 21 to 34 mM) and incubating at 37 °C for 72 h. 170 mM optimal concentration of genipin was selected as it guarantees an 80–90% of cross-linking degree with a substantial improvement in mechanical properties of SAPs and does not hinder the formation of cross-β nanofibers [31]. Functionalized SAPs were used at a concentration of 5% (w/v) [30]; multi-functionalized SAPs were tested at the concentration of 1% (w/v) [37]; BMHP1-derived peptides were dissolved at a concentration of 3% (w/v) [38]. For the optical characterization all the aforementioned peptides were used at a concentration of 0.5% (w/v). All the aforementioned peptide concentrations are above the critical concentration at which peptides show self-assembly (i.e. ~0.3% w/v).

2.3. Rheological test

Rheological properties of assembled nanostructures were carried out using a stress/rate-controlled AR-2000ex Rheometer (TA instruments) equipped with a truncated cone-plate geometry (acrylic truncated diameter, 20 mm; angle, 1°; truncation gap, 34 μm). All measurements were obtained at 25 °C using a Peltier cell in the lower

plate of the instrument to control the temperature during each test. All samples were tested one day after dissolution. Each experiment was performed in triplicate. Data were processed using Origin™ 8 software.

2.4. Thioflavin T (ThT) spectroscopy assay

ThT analysis of assembled peptides was performed to assess the presence of β-sheet fibril structures, as we previously described [37]. Measurements were done in triplicate, normalized over ThT-alone fluorescence, and processed with Origin™ 8 software.

2.5. Fourier transform infrared spectroscopy (FTIR) analysis

The FT-IR analysis of the assembled nanostructures was performed on peptides dissolved in distilled water (GIBCO®). All spectra were recorded in attenuated total reflection (ATR) using a PerkinElmer Spectrum 100 spectrometer. All the obtained spectra were reported after ATR correction, smoothing and automatic baseline correction using Origin™ 8 software. Each sample preparation was repeated three times.

2.6. Atomic force microscopy (AFM)

AFM measurements were performed in tapping mode by using a Multimode Nanoscope V system (Digital Instrument, Veeco), using single-beam silicon cantilever probes (Bruker RFESP-75 0.01–0.025 Ohm-cm Antimony (n) doped Si, cantilever f0, resonance frequency 75 kHz, constant force 3 N m^{-1}). All peptides were dissolved in distilled water (GIBCO®) a day prior to imaging. AFM images were taken by depositing 5 μl drop of peptide solutions (final concentration of 0.01% w/v) onto freshly cleaved mica. The samples were allowed to dry under ambient conditions for 5 min. Subsequently samples were rinsed with distilled water to remove loosely bound peptides, and then dried under ambient conditions for 30 min. The images were analyzed and visualized using Nanoscope Software as previously described [37].

2.7. Steady state absorption and ultrafast optical spectroscopy

Stationary absorption spectra were measured using a Jasco® V-570 UV-VIS-NIR spectrophotometer. Static photoluminescence was acquired using a Horiba® Nanolog Fluorometer (with excitation tuned from 350 nm to 550 nm, in steps of 50 nm). Absorption measurements on SAPs at different pH were performed maintaining the same 0.5% (w/v) concentration, starting from 1% concentration and adding the same amount in volume of different pH buffers. Ultrafast transient absorption (TA) experiments were performed using a Ti-Sapphire chirped pulse amplified laser (1-mJ output energy, 1-kHz repetition rate, 800 nm central wavelength, 100-fs pulse duration) [39]. For a detailed description of the TA experimental apparatus see Methods in the Supplementary information. All samples were measured at room temperature keeping the same concentration but varying the cuvette thickness according to the experiment: photoluminescence was measured in a 1 cm optical path cuvette, TA in a 1 mm optical path quartz cuvette, stationary absorption in 100 μm optical path quartz cuvette. Measurements were processed with Matlab™ 2019, and Origin™ 8 software. Global Analysis of the TA data was performed with Glotaran™ software [40].

3. Results and discussion

3.1. Cross-linking of designer self-assembly peptides

We selected a series of different SAPs comprising at least one lysine-residue per molecule to be cross-linked with genipin. All peptides name, sequences, their molecular structure, and genipin binding sites are reported in the Supplementary Table S1.

At first, we investigated six variants of the ionic self-assembling LDLK12 peptide, featuring strong propensity to spontaneously self-assemble into ordered cross-β nanofibrous structures and with proven potential for tissue engineering applications [41–43]. FAQRVPP-LDLK12 [44], SSLSVND-LDLK12 [44] and KLPGWSG-LDLK12 [45] sequences were derived from Ph.D.-7 phage library and provided functionalized microenvironments with specific biological cues coaxing adult neural stem cell (NSC) adhesion and differentiation. Both acetylated and free N-terminal versions of the above SAPs were tested to assess the contribution of a potential additional reactive group for genipin cross-linking.

We subsequently analyzed a mixture of some of the abovementioned SAPs, subsequently reinforced with LDLK12-branched peptides, acting as "molecular connector" integrated among the multifunctionalized linear SAPs (i.e. LDLK12, SSLSVND-LDLK12 and KLPGWSG-LDLK12): we selected 476 as a molar ratio between branched and linear SAPs since we previously reported it as the optimal one to have the highest increments in their storage moduli (i.e. increased overall scaffold stiffness) and intriguing neuroregenerative potential [37]. This synthetic but nature-inspired biomaterial causes a manifold increase of the stiffness, improves the β-sheet self-arrangement of LDLK12 based-sequences, fostered human neural stem cell (hNSC) maturation in 3D densely seeded cultures, and recently showed neuroregenerative potential into sub-acute spinal cord injuries [46,47].

Lastly, we explored seven Bone Marrow Homing Peptide 1 (BMHP1)-derived SAPs [38,48,49]. Biotin-GGGPFSSTKT (B3), Biotin-GGGAFSSTKT (B15), Biotin-GGGAFASTKT (B24), Biotin-GGGPFASTKT (B26), and Biotin-GGGAFASAKA (B42) peptides feature a N-terminal Biotin-tag to foster self-assembly, while Ac-WGGGAFASTKT (30) and Ac-WGGGAFSSTKT (31) peptides are just N-terminal acetylated. This ensemble of SAPs displayed a wide range of different self-assembly propensities, ranging from absent (for B26) to medium (for 30, 31) and high ones (for B3, B15, B24, and B42) [38,50]. Also, in solid-state Nuclear Magnetic Resonance (NMR) spectroscopy experiments their properties at the atomic-scale (such as mechanics, mobility and polydispersity) were efficiently correlated to their pro-adhesion and differentiation effects on neural stem cells, suggesting intriguing design strategies for tissue engineering therapies in the near future [51]. All SAP samples looked transparent before cross-linking.

3.2. Mechanical properties and nanoarchitecture of peptide networks

In the case of nanostructured hydrogels, the usual biomechanical features to be characterized are the storage (G') and loss (G'') moduli. The former reflects the stiffness trend of the biomaterial, while the latter represents the energy dissipated during the test and correlates with the liquid-like response of the hydrogel. The ratio between G' and G'' provides insights on the viscoelastic profile of tested material, allowing for the characterization of viscous-liquid ($G' < G''$) and/or elastic-solid ($G' > G''$) materials. Accordingly, sol-gel transition and mechanical behavior (with and without genipin cross-linking) have been probed using oscillatory stress rheology [30].

For all tested peptides, genipin did not influence their assembling propensity: self-assembly is usually a fast process under standard conditions (final macroscopic hydrogelation may be a matter of a few seconds), while cross-linking is much slower (from a few hours to days) [29,30].

In the gel phase, phage-derived functionalized SAPs with (full dots) and without (empty dots) genipin cross-linking (Fig. 1a) showed a G' profile almost unchanged along the tested frequency range (0.1–100 Hz), and displayed a hydrogel-like behavior with $G' > G''$ (Supplementary Fig. S2). However, the assembled functionalized SAPs without genipin are held together by non-covalent interactions (mainly by electrostatic attractions, H-bonds, and hydrophobic forces), displaying a G' profile typical of soft scaffolds [52]. Indeed, the storage modulus of FAQ$(LDLK)_3$, SSL$(LDLK)_3$, and KLP$(LDLK)_3$ ranges from 0.7 to 8 kPa: as expected, the G' value of N-terminal acetylated peptides is

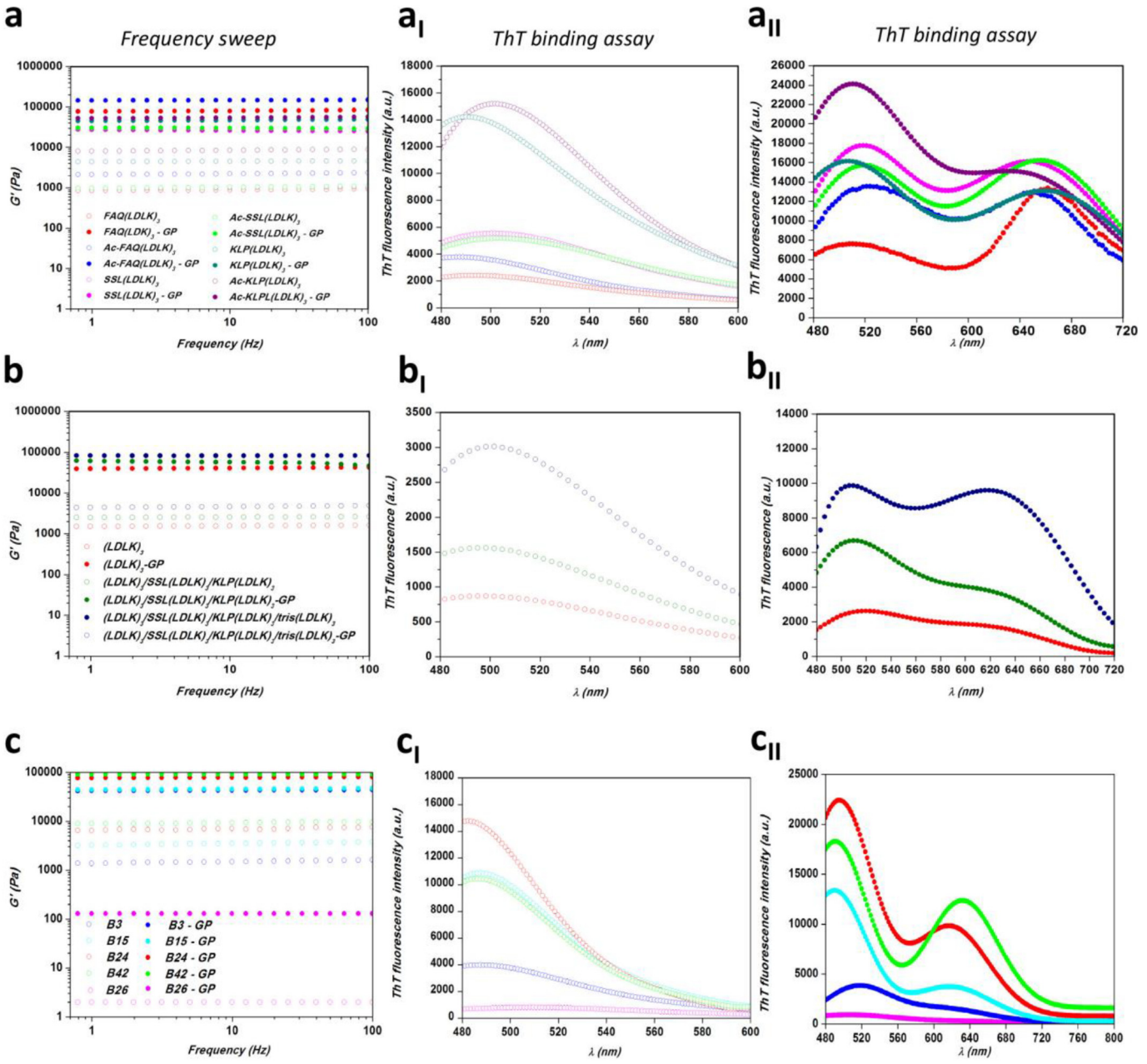

Fig. 1. Mechanical property and amyloid-like fibrillar assembly of different variants of SAPs. Dynamic frequency sweep of (a) functionalized LDLK12 peptides (5% w/v), (b) different SAP mixtures composing the final multi-functionalized hydrogel (1% w/v), (c) BMHP1-derived SAPs (3% w/v), with (full dots) and without (empty dots) genipin cross-linking, recorded as a function of angular frequency (0.1–100 Hz) at a fixed strain of 1%. (a_I, b_I, c_I) ThT emission spectra of hydrogels without genipin; all tested SAPs show amyloid-binding emission signal (peak centered at 490 nm) highlighting the β-rich nature of hydrogels. (a_{II}, b_{II}, c_{II}) ThT emission spectra of genipin cross-linked hydrogels; genipin covalent cross-linking (peak at 630 nm) does not negatively interfere on β-sheet fibril structures composing SAPs. Rather, ThT fluorescence emission further increases after cross-linking, thanks to the genipin cross-links fastening the β-structured nanofibers.

approximately 1-fold higher than their free-N-terminal counterparts as acetylation favors self-assembly of SAPs and stabilizes the assembled nanofibers [53]. By contrast, the addition of genipin cross-links inside the assembled bundles impacts on the elastic properties of the SAP hydrogels. After genipin cross-linking, G' values are increased by 50-to-100 times. The effect of the cross-linking reaction becomes most relevant on FAQ$(LDLK)_3$ and Ac-FAQ$(LDLK)_3$ peptides, featuring G' of 80 kPa and 0.2 MPa respectively, while for SSL$(LDLK)_3$, and KLP$(LDLK)_3$ display G' profiles ranging from 26 to 54 kPa.

Also, keeping in mind that nanoarchitecture and mechanical properties of nanomaterials are strictly correlated [30,37], we used the ThT-binding assay to characterize the network structure of standard (Fig. 1a_I) and cross-linked SAPs (Fig. 1a_{II}). As expected, FAQ $(LDLK)_3$, SSL$(LDLK)_3$, and KLP$(LDLK)_3$ peptides showed affinity for ThT due to the presence of cross-β fibril structures. Interestingly, genipin covalent cross-linking (peak at 630 nm) does not negatively interfere on the cross-β structures comprising the SAP nanofibers: cross-β structures are actually favored (increased peak intensity at ~490 nm) in both standard and acetylated SAPs, suggesting that genipin-mediated cross-linking acts as a "molecular fastener" preserving the previously self-assembled load-bearing nanofibrous networks, but capable of enhancing their overall mechanical properties. These data are further supported by X-ray diffraction analyses (XRD) (see Supplementary Fig. S3), where the strong peak centered at 0.45 nm was ascribable to the typical peptide backbone distance in β-sheets [30].

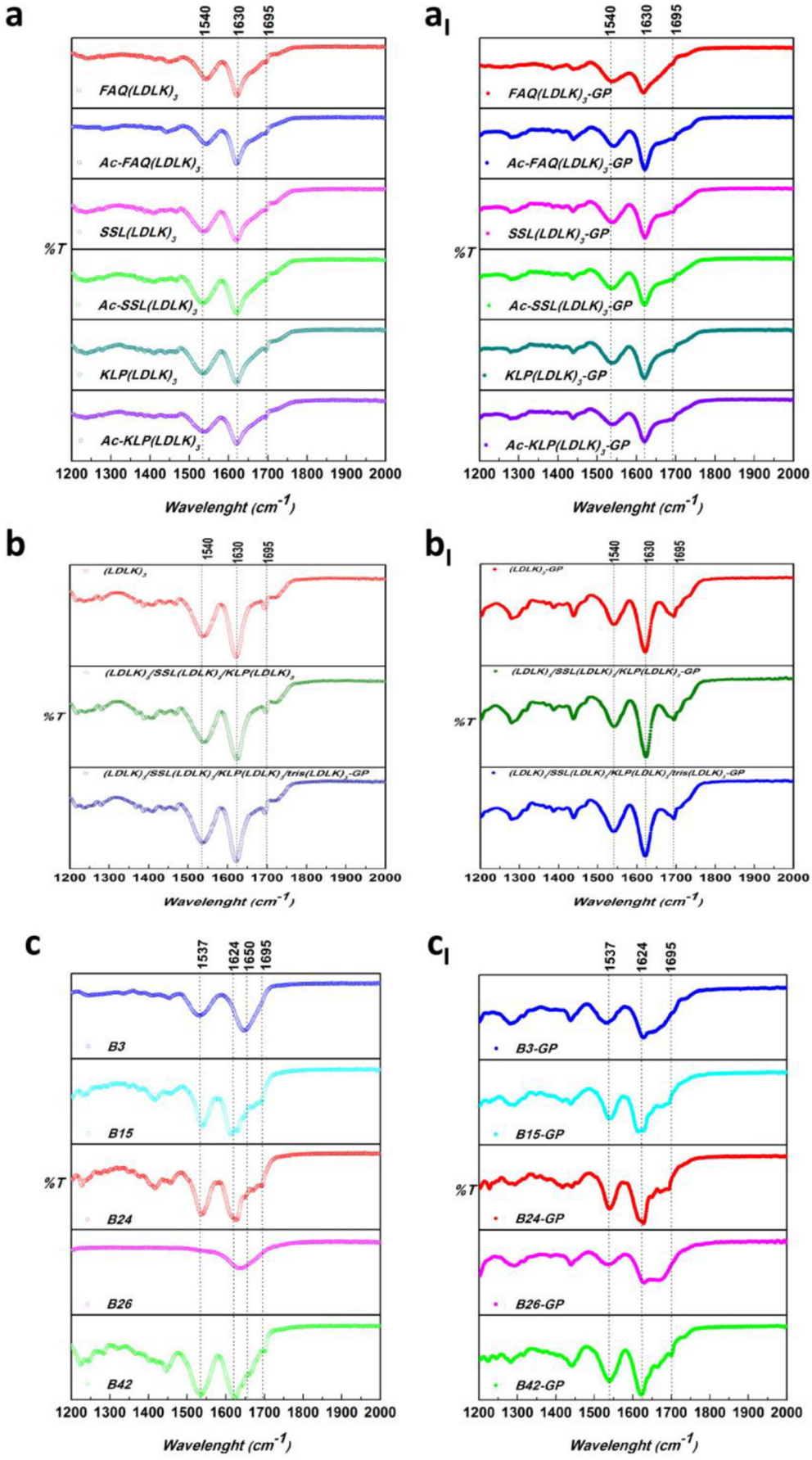

Fig. 2. Supramolecular organizations of assembled peptides. FTIR analysis of (a) functionalized LDLK12 peptides, (b) multi-functionalized peptides, and (c) BMHP1-derived peptides without genipin showing the presence of anti-parallel β-sheet assemblies. (a_I, b_I, c_I) Native β-sheet arrangements of all SAPs are all maintained after genipin cross-linking (column i).

Similarly, we probed the mechanical behavior of the multi-functionalized SAP, dubbed $(LDLK)_3$/SSL$(LDLK)_3$/KLP$(LDLK)_3$/tris$(LDLK)_3$ (Fig. 1b). Firstly, we tested the stiffening response of the different SAP mixtures composing the final hydrogel (empty dots) to gain insight on how cross-links may act on each of them. $(LDLK)_3$, $(LDLK)_3$/SSL$(LDLK)_3$/KLP$(LDLK)_3$, and $(LDLK)_3$/SSL$(LDLK)_3$/KLP$(LDLK)_3$/tris$(LDLK)_3$ hydrogels exhibited a typical viscoelastic profile with minimal G' modulus of 1.5, 2, and 4 kPa, that was starkly increased after cross-linking (full dots). Noteworthy, the G' modulus of $(LDLK)_3$/SSL$(LDLK)_3$/KLP$(LDLK)_3$/tris$(LDLK)_3$ was about 80-fold higher ($G' = 83$ kPa) after cross-linking, revealing a trend similar to that one observed in FAQRVPP-$(LDLK)_3$, albeit used at lower peptide concentration (1% w/v). Indeed, as previously reported [37], branched-SAPs act as "molecular connectors" capable of integrating within self-assembled nanostructures of linear peptides, causing a manifold increase of the assembled hydrogel stiffness (proportional to the number of self-assembling branches) with no detrimental effect on linear SAP self-assembly propensity. Indeed, in the ThT binding assay the multi-functionalized SAPs with branched tris$(LDLK)_3$ (Fig. 1b_I) showed the highest increments of ThT fluorescence values, that increased the most after cross-linking (Fig. 1b_{II}). Therefore, genipin may efficiently enhance both mechanical properties and the overall presence of cross-β structures in multi-functionalized linear/branched SAP hydrogels as well.

Finally, we probed the abovementioned theory underlying genipin cross-linking in SAPs featuring different backbone chain sequences, length, and self-structuration (Fig. 1c). We selected different self-assembling variants of the BMHP1-derived SAPs (see Section 3.1 for further details). Self-assembled hydrogels of peptides B3, B15, B24, and B42 (Fig. 1c, empty dots) showed typical hydrogel-like profiles, featuring a predominantly elastic solid-like behavior with G' of 1.5, 3.6, 7 and 9.5 kPa, respectively, while peptides B26, 30, and 31 (Fig. 1c and Supplementary Fig. S4a) showed viscous-liquid properties (G' near to zero), implying a weaker tendency to assemble. In contrast, the addition of genipin cross-links inside the BMHP1-derived SAP assembled bundles, triggered G' increments from 43 to 68 kPa for B3, B15, B24, and B42 (Fig. 1c, full dots). Notably, cross-linked B26 displayed an elastic-solid profile with increased storage moduli ($G' > 100$ Pa) and similarly, 30 and 31 showed G' values well above 2 kPa. In this case too, the ThT assay, probing β-sheet presence, showed higher values for cross-linked SAPs (Fig. 1c_I, c_{II} and Supplementary Fig. S4a_I, a_{II}). To further reinforce our hypothesis, we showed that genipin cross-linking takes place also with SAPs featuring two well-interspaced lysines (Supplementary Fig. S5a), while no cross-linking occurred for a SAP with no lysines (Supplementary Fig. S5b).

In addition to the stiffening behavior of cross-linked samples, stress-to-failure tests were also performed to assess failure when subjected to a linear strain/stress progression. Cross-linking of peptide chains yielded to overall failure-stress increments (final values up to 3.5 kPa, Supplementary Fig. S6) compared to standard hydrogels [29,30,37].

Moreover, interestingly the obtained G' values of cross-linked FAQRVPP-$(LDLK)_3$ (0.2 MPa; at 5% w/v), $(LDLK)_3$/SSL$(LDLK)_3$/KLP$(LDLK)_3$/tris$(LDLK)_3$ (83 kPa; 1% w/v), and B42 (68 kPa; 3% w/v), considerably higher than those of other SAP-based hydrogels [25,54,55], fall within the range of various biological tissues [56], and, therefore may constitute an appropriate match for their regeneration. Lastly, the same cross-linked SAPs may be used as stiff but wet components in seals, conductors, sensors, and actuators [57,58].

3.3. Supramolecular organizations of assembled peptide networks

The supramolecular nanoarchitecture of assembled peptide networks was also pursued by ATR FT-IR spectroscopy. In the Amide I region (1600–1700 cm^{-1}), mainly associated with different C═O stretching vibrations in secondary structures of peptides/proteins, both mono-functionalized (Fig. 2a) and multi-functionalized (Fig. 2b) SAP-samples showed anti-parallel β-sheet features characterized by the presence of the two components at 1630 and 1695 cm^{-1} [59]. The β-sheet aggregation was also confirmed by the peak at 1540 cm^{-1} in the Amide II region (1480–1575 cm^{-1}), directly related to CN stretching and NH bending. Predominantly anti-parallel β-sheet features were also observed in cross-linked SAPs (Fig. 2a_I, b_I), but with a ~10% higher β-sheet organizational index (ratio of the peak intensities at 1695 cm^{-1} and 1630 cm^{-1}, proportional to the ratio of antiparallel/parallel β-sheet structures) [60].

FT-IR spectra of standard BMHP1-derived SAPs showed variations of their supramolecular organization correlated to their different self-assembly propensity (Fig. 2c). B26 hydrogel, in line with its poor self-assembly propensity, gave a shapeless spectrum typical of unordered aggregated strands. On the contrary, Amide I, and Amide II region of B3 showed peaks at 1650 cm^{-1} and 1537 cm^{-1} respectively, testifying its high content of β-turn/random coil conformers. In stark contrast, B15, B24, and B42 hydrogels showed intense peaks at 1624 and 1695 cm^{-1} (β-sheet organizational index = 36.6%), featuring strong anti-parallel β-sheet aggregation. Notably, in both B3-GP and B26-GP hydrogels, peaks at 1624 cm^{-1} (in the Amide I region) and at 1537 cm^{-1} (in the Amide II region), ascribable to β-sheet structures, were clearly visible (Fig. 2c_I). This observation highlights that genipin cross-links could switch supramolecular structures of B26 and B3 peptides from unordered (or more complex) aggregated strands to ordered β-sheet structures. Conversely, hydrogels B15, B24, and B42 cross-linked with genipin still maintained anti-parallel β-sheet patterns, with a β-sheet organizational index of 45%. Native β-sheet

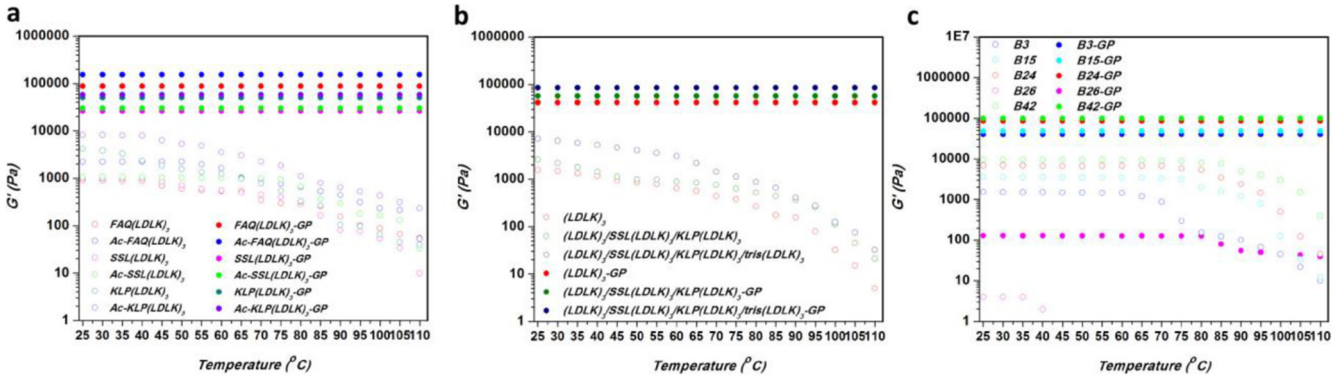

Fig. 3. Thermo-mechanical stability of assembled cross-linked peptides. Thermo-mechanical analysis of (a) functionalized LDLK12 peptides, (b) multi-functionalized peptides, and (c) BMHP1-derived peptides before (empty dots) and after genipin cross-linking (full dots): G' measurement during a temperature ramp (25–110 °C). Above temperatures ranging from 25 to 80 °C the slope of G' of standard SAPs drastically decreases, suggesting a gel-sol transition of all hydrogels. Conversely, the G' profile of genipin cross-linked SAPs steadily withstands the heating ramp, showing preserved stiffness throughout the tested range of temperatures.

arrangements of peptides 30 and 31 were also maintained after cross-linking (Supplementary Fig. S7). These findings strongly indicate that genipin cross-links play a key role in the formation of ordered and rigid BMHP1-derived scaffolds, maintaining (in case of already structured SAPs) or boosting (in case of poorly self-assembling peptides) the β-structuration of the already assembled supramolecular structures.

Altogether, FT-IR analysis confirmed the self-aggregation of all tested SAPs into β-sheets, suggesting that the introduction of genipin cross-links in the assembled bundles did not impair the β-sheet formation propensity of the tested SAP hydrogels.

3.4. Tuning thermo-mechanical stability

We previously demonstrated that genipin cross-linking increases the bioabsorption time of functionalized self-assembling peptides in vitro [30]: we here assessed the thermo-mechanical properties of SAPs before (empty dots) and after genipin cross-linking (full dots) by measuring G' throughout a temperature ramp (25–110 °C) (Fig. 3a, b, c) (see Methods for details). Above temperatures ranging from 25 to 40 °C (for LDLK12-based SAPs) or 35–80 °C (for BMHP1-derived SAPs), the slope of G' of standard SAPs drastically decreased, suggesting a gel-sol transition of all hydrogels concurrently with a substantial loss of their viscous-elastic properties. On the other hand, the G' profile of genipin cross-linked SAPs steadily withstood the heating ramp, remaining constant within the tested temperature range. Unlike most of SAP-hydrogels [61], cross-linked gels showed preserved stiffness throughout the tested broad temperature ramp. For the sake of completeness, data trends were also confirmed by using a parallel plate geometry (see Supplementary methods and Supplementary Fig. S8). This change strongly points out the resistance of the genipin covalent links to thermal denaturation and, most importantly, their strong contribution to the overall thermal resistance of the cross-linked β-sheets comprising the nanofibrous hydrogels. This remarkable property ascribable to genipin cross-links was also observed by Pan et al. [62]: they cross-linked layer-by-layer the positively charged polyethylenimine (PEI) and negatively charged hypophosphorous acid-modified chitosan (HACH) on cotton fabric, demonstrating that uniformly dispersed genipin can significantly increase the thermal stability of coated cotton fabric compared with untreated samples.

In summary, genipin cross-linking enhanced the mechanical properties of the tested SAPs, but also their thermo-stability up to and beyond 100 °C.

3.5. Morphological studies

Morphological characterization of assembled SAP networks was undertaken via Atomic force microscopy (AFM) (Fig. 4). For simplicity, we reported SAPs data that showed better performance in terms of stiffness and β-sheet packing increments.

AFM of peptide FAQ$(LDLK)_3$ (Fig. 4a) showed short and single fibers (height ~0.8 nm, Supplementary Fig. S9a; width ~13.37 ± 4.20 nm, Supplementary Fig. S10a–b), comparable to previously obtained data [30]. Instead, genipin cross-linked FAQ$(LDLK)_3$ assembled into a uniform tight and clustered bundle network of cross-linked nanofibers (Fig. 4a) (height ~1.6 nm, Supplementary Fig. S9b; width ~19 ± 3.5 nm, Supplementary Fig. S10c–d). Hence, average nanofibers height of cross-linked SAP is ~1 fold bigger, while width is ~6 nm bigger if compared to FAQ$(LDLK)_3$.

AFM (Fig. 4b) data of multi-functionalized SAP showed that both $(LDLK)_3$/SSL$(LDLK)_3$/KLP$(LDLK)_3$/tris$(LDLK)_3$, with and without genipin cross-linking, assemble into homogeneous nanofibers. The $(LDLK)_3$/SSL$(LDLK)_3$/KLP$(LDLK)_3$/tris$(LDLK)_3$ height was ~1.25 nm (Supplementary Fig. S9c), while after genipin cross-linking it was ~1.9 nm (Supplementary Fig. S9d). In agreement with previously published data [37], average fiber width was 7.22 ± 2.5 nm (Supplementary Fig. S11a–b) and 23.62 ± 6.58 nm (~16 nm bigger, Supplementary Fig. S11c–d) for $(LDLK)_3$/SSL$(LDLK)_3$/KLP$(LDLK)_3$/tris$(LDLK)_3$ before and after cross-linking respectively.

Finally, we explored morphological properties of BMHP1-derived SAPs (Fig. 4c). B42 peptide assembled into uniform long and flat nanofibers (Fig. 4d) (height ~1.13 nm, Supplementary Fig. S9e; width = 20.62 ± 5.8 nm, Supplementary Fig. S12a–b) in agreement with previous studies [48]. Contrarily, AFM data showed that B42 peptide cross-linked with genipin exhibited markedly different nanofibers morphology, featuring thicker and left-handed twisted nanofibers (Fig. 4e). Nanofibers height was around 5 nm (Supplementary Fig. S9f), while width was 40.7 ± 5.23 nm (Supplementary Fig. S12c–d), the bigger features being ascribable to fibers clamped together by genipin cross-links. The detected height and width changes between not cross-linked and cross-linked SAPs, together with FT-IR data, suggest that genipin covalent bonds mainly connect already self-assembled nanostructures, acting at the nano- and micro-structural levels, and minimally affecting SAP secondary structure arrangements. As such, the theories developed so far for SAPs to warrant proper biomimetic and self-assembling properties [2] are still valid for genipin cross-linked SAPs.

3.6. Optical characterization

We performed stationary and transient optical characterization of the two SAPs displaying the most dramatic changes after cross-linking: B42 and the multi-functionalized $(LDLK)_3$/SSL$(LDLK)_3$/KLP$(LDLK)_3$/tris$(LDLK)_3$ peptide. Fig. 5a shows the linear absorption spectra of the genipin molecule alone (red dots), of B42 before (light green dots) and after the genipin cross-linking (green line) and of the multi-functionalized SAP without (light green dash-line) and with genipin cross-linking (blue dash-line). The inset is a zoom in the visible spectral range of the linear absorption spectra.

Cross-linking deeply modified the absorption spectrum of both SAPs. A direct comparison with the genipin spectrum showed that the band at 240 nm could be assigned to the genipin moiety, while the absorption below 220 nm was due to the peptide backbone. The other transitions at longer wavelengths (360 nm, 450 nm, and 600 nm) were present only in the cross-linked samples and thus were correlated to their structural characteristics. In the wavelength range between 300 nm and 450 nm, similar transitions (and corresponding emissions) have already been observed in β-sheet-rich peptide aggregates [63–65]. They were tentatively assigned to networks of hydrogen bonds connecting different protofibrils, promoting charge delocalization through proton transfer (Fig. 5b, light blue clouds). In our samples, the increased nanofibrils order bestowed by cross-linking likely enhanced these transitions [66]. Another clear band, peaking at 600 nm, was detected in the cross-linked samples: we assigned it to a newly formed electronic state, directly connected to the genipin covalent bonding between peptide chains. This band was indeed present in both the cross-linked B42 and $(LDLK)_3$/SSL$(LDLK)_3$/KLP$(LDLK)_3$/tris$(LDLK)_3$ samples (inset in Fig. 5a), with similar spectral position and intensity. There was actually a slight red shift of a few nanometers and a peak broadening in $(LDLK)_3$/SSL$(LDLK)_3$/KLP$(LDLK)_3$/tris$(LDLK)_3$ peptide, which we tentatively justified with the presence of more linking points (if compared to B42) between the SAP chains (red clouds in Fig. 5b), and to the higher complexity of the supramolecular configuration of the fibrils of the multi-functionalized SAP [37]. We also performed static photoluminescence of the cross-linked peptides: the emission spectra with excitation from 350 nm to 550 nm are shown in Fig. S13. We detected three different emissive states peaked at ~450 nm, 510 nm, and 610–620 nm. These states showed different ratio of intensity for the two SAPs, giving a second confirmation of the differences in their supramolecular organization (due to cross-linking and aggregation degrees) and distribution of energy levels. The shorter wavelength emissive peaks are related to the absorption bands at 360 nm and 450 nm, and their large Stokes shift is consistent with previous results [65]. The emission at 610–620 nm, instead, presented a smaller Stokes shift: this is a further

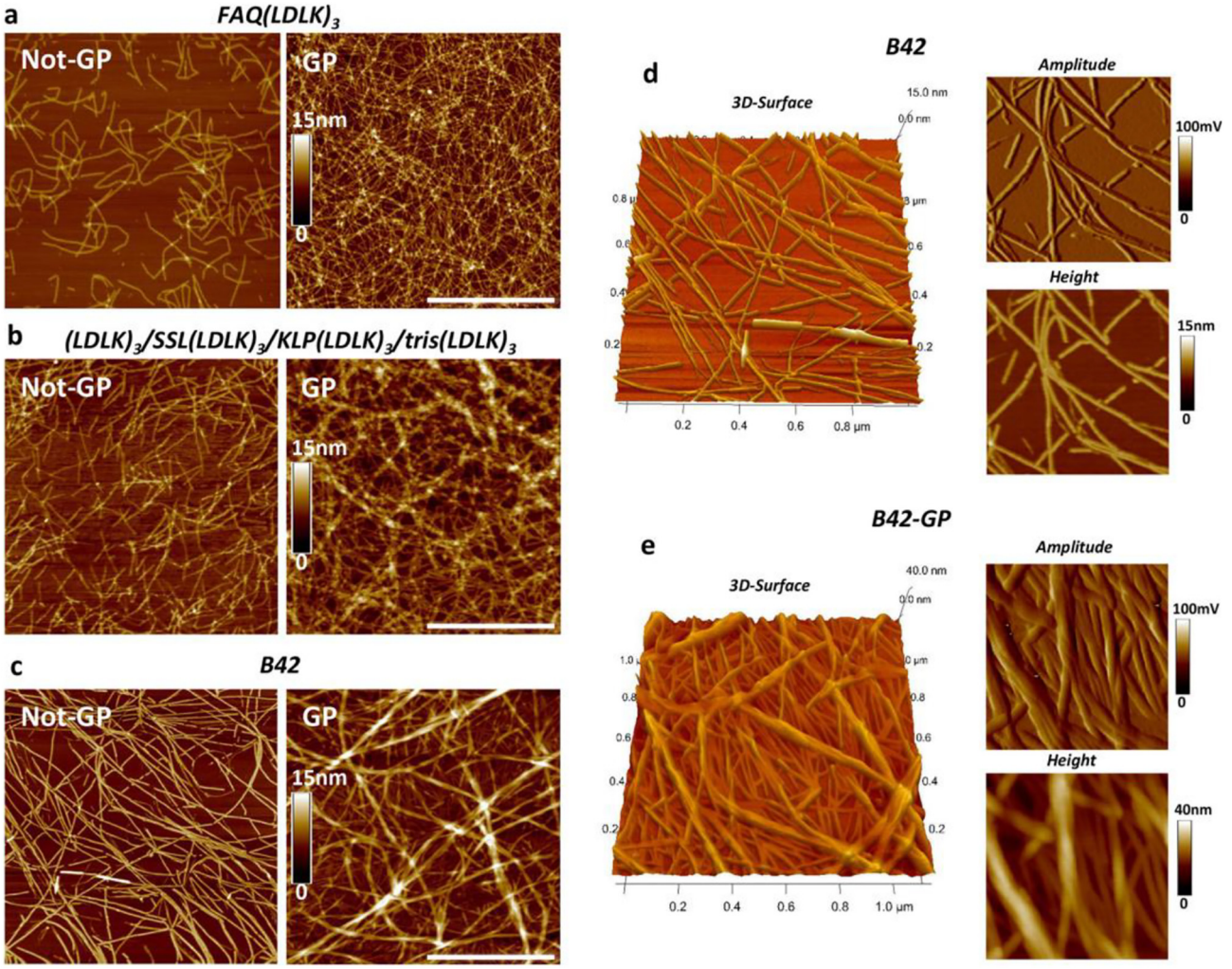

Fig. 4. Atomic force microscopy (AFM) studies. AFM images of (a) FAQRVPP-$(LDLK)_3$, (b) $(LDLK)_3$/SSL$(LDLK)_3$/KLP$(LDLK)_3$/tris$(LDLK)_3$, and (c) B42 peptides fibers with and without genipin cross-linking (scale bar is 1 μm). 3D surface, amplitude, and height of B42 peptide high-magnification images, (d) without and (e) with genipin cross-linking. B42 peptide assembles into uniform long, and flat nanofibers; contrarily, peptide B42 with genipin self-organize into thicker and left-handed twisted nanofibers.

confirmation of the novel nature of the absorption band peaked at 600 nm.

To further confirm the nature of these transitions, both SAPs have been characterized for different values of the buffer pH. Looking at the B42 absorption (Fig. 5c), the transitions related to the backbone and the genipin ring were unchanged for all pH values except for pH 14, where a drastic shift of the 240 nm transition could be assigned to a breaking of the genipin ring [67]. The transitions between 250 nm and 450 nm displayed stronger pH dependence due to the modification of the H-bonds, confirming the previous assignment [66]. On the other hand, the transition around 600 nm followed a different trend. For pH values closer to the buffer neutrality, spectra were all similar, while the ones at pH 2 and pH 10 were slightly red shifted. This shift usually happens for transitions possessing a charge transfer (CT) character [68,69]. Hence the optical transition at 600 nm corresponds to an electronic excited state configuration where the electrons and holes are spatially separated from each other, creating a local distribution of delocalized charges. Therefore, CT states are sensitive to the charged solvent environment in which the molecular complex is dissolved. In the cross-linked B42, the CT state is delocalized across the genipin and it is sensitive to charge-environment variations induced by highly basic or acidic buffers. Going towards more basic buffers (pH 12 and 14) the 600 nm transition started to blue shift and eventually lost intensity due to the known breaking of the genipin ring [67], thus giving a confirmation that the 600 nm absorption band is related to the covalent bonding of the peptide chains through the genipin molecule. Fig. 5d reports the pH dependence of the absorption spectrum for $(LDLK)_3$/SSL$(LDLK)_3$/KLP$(LDLK)_3$/tris$(LDLK)_3$: the spectral shift of the CT state was less clear likely due to the higher complexity of the self-assembled nanostructures.

The presence of a transition in the visible was very interesting, since polypeptides and proteins typically absorb in the UV only, in the 250–300 nm band (for the aromatic amino acids) and at wavelengths shorter than 250 nm (for the polypeptide backbone). The observation of visible absorption and fluorescence paves the way to novel biocompatible, pH-sensitive and biodegradable fluorophores to be potentially used in biomedical imaging, optoelectronic and photonic devices.

Consequently, we have investigated the ultrafast dynamics of this visible transition using femtosecond transient absorption (TA) spectroscopy. In this technique an ultra-short (~100-fs duration) pump pulse photoexcites the sample and a time-delayed broadband probe pulse measures the pump-induced absorption change ΔA. In our experiment the pump pulse was tuned to 400 nm, resonant with one of the transitions of the SAPs formed only in presence of genipin, with the probe covering the 450–750 nm wavelength range. Fig. 5e and f shows 2D ΔA maps, as a function of probe wavelength and pump-probe delay, for B42 and $(LDLK)_3$/SSL$(LDLK)_3$/KLP$(LDLK)_3$/tris$(LDLK)_3$ respectively. Negative signals, identified by red color, were assigned to Ground

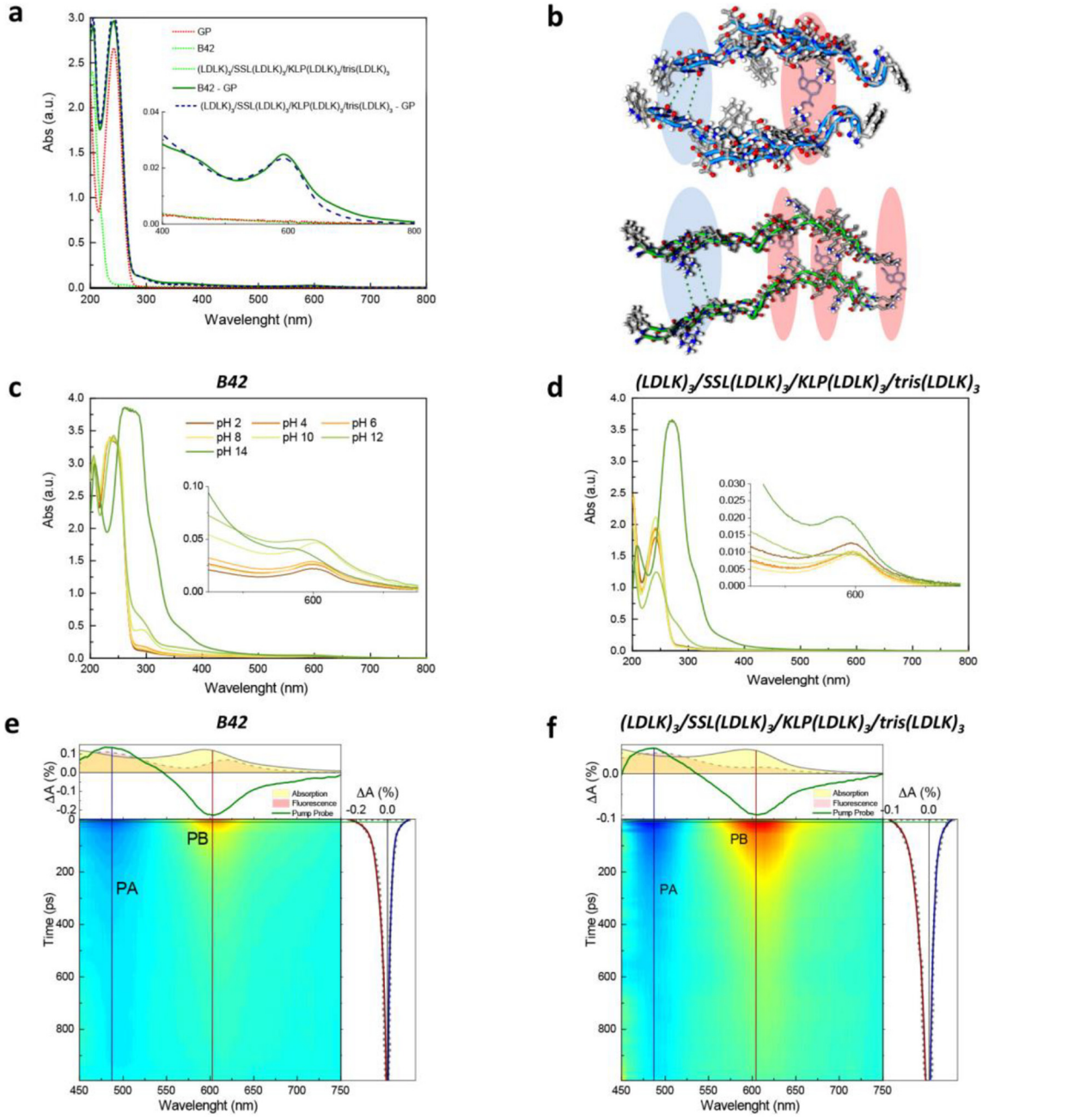

Fig. 5. Static and transient optical characterization. Static absorption (a) of B42 and multi-functionalized peptides without (green dots) and with genipin cross-linking (green and blue line) compared with the one of genipin itself (red dots). The inset is a zoom in the visible spectral range of the linear absorption spectra showing peak at 600 nm, detected only in the cross-linked samples. We assigned it to a newly formed electronic state, directly connected to the covalent bonding between the chains due to genipin. (b) Schematic representation of the cross-linked SAPs along with the parts of the molecules mostly involved in the optical transitions, namely the CT state-like (red clouds) and the H-bond induced transition (blue clouds). Absorption spectra of both (c) B42 and (d) multi-functionalized peptide tested at different pH values. Transient absorption data of (e) cross-linked B42, and (f) cross-linked multi-functionalized peptide. The ΔA maps in time and wavelength are shown with corresponding cuts in time (spectrum at 2 ps, green line in the top panel) and in wavelength (dynamics at 485 nm, dark blue line, and at 602–604 nm, dark red line, in the side panel). In the top panel of both (e) and (f) the absorption spectra (yellow) and fluorescence spectra (orange) of the SAPs are shown for comparison with the ΔA signal.

State Bleaching (GSB), i.e. reduction of the sample absorption due to photoexcitation of the electronic transition, and/or to Stimulated-Emission (SE) from the excited state. Positive signals, identified by blue color, corresponded to photo-induced absorption, i.e. decreased transmission of the probe pulse. For clearer identification of these signals, we reported in the upper panels of both Fig. 5e and f the ΔA spectra (at 1-ps pump-probe delay) together with the absorption (yellow) and photoluminescence (orange, with excitation at 400 nm) spectra of the corresponding samples. The negative band centered at around 600 nm corresponded to the superposition of GSB and SE from the photoexcited electronic transition. The blue-shifted positive band peaking at 485 nm (excited state absorption) could be assigned either to a higher lying state or to a blue shift of the ground state absorption spectrum induced by the photoexcited charges: this phenomenon, known as photoinduced stark effect [70–72], could be a further confirmation of the CT nature of the transition.

The side panels of Fig. 5e–f report two ΔA time traces at wavelengths corresponding to positive (dark blue, 485 nm) and negative (dark red,

600 nm ca.) peaks of the ΔA spectrum. Global analysis of the ΔA dynamics according to a sequential model reveals a bi-exponential decay with two-times decay constants. The obtained time constants are reported in Table S2, while the corresponding Evolution Associated Spectra (EAS) of the two sequential excited species are shown in Fig. S14. The first time constant ($\tau_1 < 50$ ps) could be assigned to relaxation from the photoexcited bright state to the CT state and the second one ($\tau_2 > 200$ ps) to the ground state recovery. This interpretation was confirmed by the change of shape from the first EAS (EAS-τ_1) to the second one (EAS-τ_2), showing a red shift around 600 nm, which corresponds to the formation of SE from the CT state after the first relaxation. The dynamics of $(LDLK)_3$/SSL $(LDLK)_3$/KLP$(LDLK)_3$/tris$(LDLK)_3$ peptide showed time constants approximately one third longer than in B42 (see Table S2 for time constants values). This was likely ascribable to different chain interactions in the peptide network, resulting in a stronger delocalization of the excitation, or to a higher probability of trap states formation [73,74], yielding to a slower relaxation path of the electrons towards the ground state. This behavior is also confirmed by the different shapes and intensity ratio of the peaks in the emission spectra (see Fig. S8). In the B42 cross-linked sample, the strong intensity of the emission around 620 nm is a consequence of the faster relaxation of the excitation towards this lower energy state. Instead, the presence of highly emissive intermediate states between the excitation at 400 nm and the transition at 600 nm in the $(LDLK)_3$/SSL$(LDLK)_3$/KLP$(LDLK)_3$/tris$(LDLK)_3$ cross-linked peptide (shown by the higher relative intensity of emission around 450 nm and 510 nm) is strictly related to the slower relaxation decay of the excitation observed in the pump probe experiments.

4. Conclusions

Overall genipin cross-linking featured the great advantage of being effective with very different lysine-containing SAP hydrogels, without altering their secondary structure and nanofibrous morphology, both critical for many biomedical applications (e.g. biomimetic scaffolds, drug release, etc.). Presumably, this cross-linking approach may offer the opportunity to fine-tune any β-sheet forming SAP featuring at least one lysine residue, or other more complex proteinaceous materials, yielding to stiffer and more thermostable biomimetic hydrogel scaffolds. Lastly, genipin cross-linking, changing the absorption/emission bands in the visible range and the kinetic of relaxation of a variety of SAPs, may bestow a promising unexplored potential in biomedical imaging, photonics [75], optoelectronics [76], power harvesting [77] to several well-known and new SAPs, resulting in potentially novel biocompatible and pH-sensitive fluorophores [63].

Funding sources

The work described and performed by R.P., and F.G. was funded by "Ricerca Corrente 2018-2020" funding granted by the Ministry of Health, Italy and by the "5 × 1000" voluntary contributions. Financial support also came from Revert onlus.

CRediT authorship contribution statement

Raffaele Pugliese: Conceptualization, Methodology, Formal analysis, Validation, Data curation, Investigation, Supervision, Project administration, Writing - original draft, Writing - review & editing. **Luca Moretti:** Methodology, Validation, Formal analysis, Investigation, Data curation, Writing - original draft. **Margherita Maiuri:** Data curation, Writing - review & editing. **Tiziana Romanazzi:** Validation. **Giulio Cerullo:** Supervision, Writing - original draft, Writing - review & editing. **Fabrizio Gelain:** Conceptualization, Formal analysis, Funding acquisition, Supervision, Project administration, Writing - original draft, Writing - review & editing.

Declaration of Competing Interest

The authors declare that they have no known competing for financial interests or personal relationships that could have appeared to influence the work reported in this paper.

Acknowledgment

We are grateful to Prof. Luca Beverina for allowing our FTIR experiments to be performed at his facility at the Material Science Department of the University of Milan-Bicocca.

Appendix A. Supplementary data

The following files are available free of charge: Materials and methods; genipin cross-linking reaction scheme; self-assembling peptides structures; HPLC and LC-MS spectra of self-assembling peptides; X-ray diffraction; biomechanics assessment of different cross-linking SAPs; FT-IR analysis; AFM morphological analysis, static photoluminescence spectra. Supplementary data to this article can be found online at https://doi.org/10.1016/j.matdes.2020.108901.

References

[1] K. Kinbara, T. Aida, Toward intelligent molecular machines: directed motions of biological and artificial molecules and assemblies, Chem. Rev. 105 (4) (2005) 1377–1400.
[2] R. Pugliese, F. Gelain, Peptidic biomaterials: from self-assembling to regenerative medicine, Trends Biotechnol. 35 (2) (2017) 145–158.
[3] A. Handelman, N. Lapshina, B. Apter, G. Rosenman, Peptide integrated optics, Adv. Mater. 30 (5) (2018).
[4] K. Tao, P. Makam, R. Aizen, E. Gazit, Self-assembling peptide semiconductors, Science 358 (6365) (2017).
[5] S. Zhang, Fabrication of novel biomaterials through molecular self-assembly, Nat. Biotechnol. 21 (10) (2003) 1171–1178.
[6] F. Gelain, S. Panseri, S. Antonini, C. Cunha, M. Donega, J. Lowery, F. Taraballi, G. Cerri, M. Montagna, F. Baldissera, A. Vescovi, Transplantation of nanostructured composite scaffolds results in the regeneration of chronically injured spinal cords, ACS Nano 5 (1) (2011) 227–236.
[7] E. Genove, C. Shen, S. Zhang, C.E. Semino, The effect of functionalized self-assembling peptide scaffolds on human aortic endothelial cell function, Biomaterials 26 (16) (2005) 3341–3351.
[8] X. Wu, L. He, W. Li, H. Li, W.M. Wong, S. Ramakrishna, W. Wu, Functional self-assembling peptide nanofiber hydrogel for peripheral nerve regeneration, Regenerative biomaterials 4 (1) (2017) 21–30.
[9] Y. Sun, W. Li, X. Wu, N. Zhang, Y. Zhang, S. Ouyang, X. Song, X. Fang, R. Seeram, W. Xue, L. He, W. Wu, Functional self-assembling peptide nanofiber hydrogels designed for nerve degeneration, ACS Appl. Mater. Interfaces 8 (3) (2016) 2348–2359.
[10] J. Guo, K.K. Leung, H. Su, Q. Yuan, L. Wang, T.H. Chu, W. Zhang, J.K. Pu, G.K. Ng, W.M. Wong, X. Dai, W. Wu, Self-assembling peptide nanofiber scaffold promotes the reconstruction of acutely injured brain, Nanomedicine 5 (3) (2009) 345–351.
[11] B.B. Hsu, W. Conway, C.M. Tschabrunn, M. Mehta, M.B. Perez-Cuevas, S. Zhang, P.T. Hammond, Clotting mimicry from robust hemostatic bandages based on self-assembling peptides, ACS Nano 9 (9) (2015) 9394–9406.
[12] S. Vauthey, S. Santoso, H. Gong, N. Watson, S. Zhang, Molecular self-assembly of surfactant-like peptides to form nanotubes and nanovesicles, Proc. Natl. Acad. Sci. U. S. A. 99 (8) (2002) 5355–5360.
[13] S. Alam, J.J. Panda, T.K. Mukherjee, V.S. Chauhan, Short peptide based nanotubes capable of effective curcumin delivery for treating drug resistant malaria, Journal of nanobiotechnology 14 (2016) 26.
[14] S. Gudlur, P. Sukthankar, J. Gao, L.A. Avila, Y. Hiromasa, J. Chen, T. Iwamoto, J.M. Tomich, Peptide nanovesicles formed by the self-assembly of branched amphiphilic peptides, PLoS One 7 (9) (2012), e45374. .
[15] Z.A.l. Armando Hernandez-Garcia, Dina Simkin, Ashwin Madhan, Eloise Pariset, Faifan Tantakitti, Oscar de J. Vargas-Dorantes, Sungsoo S. Lee, Evangelos Kiskinis, Samuel I. Stupp, Peptide–siRNA supramolecular particles for neural cell transfection, Adv Science (1801458) (2018).
[16] M.L. Gardel, J.H. Shin, F.C. MacKintosh, L. Mahadevan, P. Matsudaira, D.A. Weitz, Elastic behavior of cross-linked and bundled actin networks, Science 304 (5675) (2004) 1301–1305.
[17] I.K. Piechocka, R.G. Bacabac, M. Potters, F.C. Mackintosh, G.H. Koenderink, Structural hierarchy governs fibrin gel mechanics, Biophys. J. 98 (10) (2010) 2281–2289.
[18] S. Yang, S. Wei, Y. Mao, H. Zheng, J. Feng, J. Cui, X. Xie, F. Chen, H. Li, Novel hemostatic biomolecules based on elastin-like polypeptides and the self-assembling peptide RADA-16, BMC Biotechnol. 18 (1) (2018) 12.
[19] M. Ozeki, S. Kuroda, K. Kon, S. Kasugai, Differentiation of bone marrow stromal cells into osteoblasts in a self-assembling peptide hydrogel: in vitro and in vivo studies, J. Biomater. Appl. 25 (7) (2011) 663–684.

[20] B. He, Y. Ou, S. Chen, W. Zhao, A. Zhou, J. Zhao, H. Li, D. Jiang, Y. Zhu, Designer bFGF-incorporated d-form self-assembly peptide nanofiber scaffolds to promote bone repair, Mater. Sci. Eng. C Mater. Biol. Appl. 74 (2017) 451–458.
[21] A. Schneider, J.A. Garlick, C. Egles, Self-assembling peptide nanofiber scaffolds accelerate wound healing, PLoS One 3 (1) (2008), e1410. .
[22] Y. Loo, Y.C. Wong, E.Z. Cai, C.H. Ang, A. Raju, A. Lakshmanan, A.G. Koh, H.J. Zhou, T.C. Lim, S.M. Moochhala, C.A. Hauser, Ultrashort peptide nanofibrous hydrogels for the acceleration of healing of burn wounds, Biomaterials 35 (17) (2014) 4805–4814.
[23] Y. Ichihara, M. Kaneko, K. Yamahara, M. Koulouroudias, N. Sato, R. Uppal, K. Yamazaki, S. Saito, K. Suzuki, Self-assembling peptide hydrogel enables instant epicardial coating of the heart with mesenchymal stromal cells for the treatment of heart failure, Biomaterials 154 (2018) 12–23.
[24] D. Cigognini, A. Satta, B. Colleoni, D. Silva, M. Donega, S. Antonini, F. Gelain, Evaluation of early and late effects into the acute spinal cord injury of an injectable functionalized self-assembling scaffold, PLoS One 6 (5) (2011), e19782. .
[25] A. Raspa, G.A.A. Saracino, R. Pugliese, D. Silva, D. Cigognini, A. Vescovi, F. Gelain, Complementary co-assembling peptides: from in silico studies to in vivo application, Adv. Funct. Mater. 24 (40) (2014) 6317–6328.
[26] H. Yokoi, T. Kinoshita, S. Zhang, Dynamic reassembly of peptide RADA16 nanofiber scaffold, Proc. Natl. Acad. Sci. U. S. A. 102 (24) (2005) 8414–8419.
[27] Y. Zhao, H. Yokoi, M. Tanaka, T. Kinoshita, T. Tan, Self-assembled pH-responsive hydrogels composed of the RATEA16 peptide, Biomacromolecules 9 (6) (2008) 1511–1518.
[28] M.P. Hendricks, K. Sato, L.C. Palmer, S.I. Stupp, Supramolecular assembly of peptide amphiphiles, Acc. Chem. Res. 50 (10) (2017) 2440–2448.
[29] R. Pugliese, A. Marchini, G.A.A. Saracino, R.N. Zuckermann, F. Gelain, Cross-linked self-assembling peptide scaffolds, Nano Res. 11 (1) (2018) 586–602.
[30] R. Pugliese, M. Maleki, R.N. Zuckermann, F. Gelain, Self-assembling peptides cross-linked with genipin: resilient hydrogels and self-standing electrospun scaffolds for tissue engineering applications, Biomaterials science 7 (1) (2018) 76–91.
[31] M.A. Khalily, M. Goktas, M.O. Guler, Tuning viscoelastic properties of supramolecular peptide gels via dynamic covalent crosslinking, Organic & Biomolecular Chemistry 13 (7) (2015) 1983–1987.
[32] V.A. Kumar, S. Shi, B.K. Wang, I.C. Li, A.A. Jalan, B. Sarkar, N.C. Wickremasinghe, J.D. Hartgerink, Drug-triggered and cross-linked self-assembling nanofibrous hydrogels, J. Am. Chem. Soc. 137 (14) (2015) 4823–4830.
[33] S. Boothroyd, A. Saiani, A.F. Miller, Controlling network topology and mechanical properties of co-assembling peptide hydrogels, Biopolymers 101 (6) (2014) 669–680.
[34] Y. Li, L. Li, C. Holscher, Therapeutic potential of genipin in central neurodegenerative diseases, CNS Drugs 30 (10) (2016) 889–897.
[35] G. Chen, X. Guo, Neurobiology of Chinese herbal medicine on major depressive disorder, Int. Rev. Neurobiol. 135 (2017) 77–95.
[36] W. Xiao, S. Li, S. Wang, C.T. Ho, Chemistry and bioactivity of Gardenia jasminoides, J. Food Drug Anal. 25 (1) (2017) 43–61.
[37] R. Pugliese, F. Fontana, A. Marchini, F. Gelain, Branched peptides integrate into self-assembled nanostructures and enhance biomechanics of peptidic hydrogels, Acta Biomater. 66 (2018) 258–271.
[38] F. Gelain, D. Silva, A. Caprini, F. Taraballi, A. Natalello, O. Villa, K.T. Nam, R.N. Zuckermann, S.M. Doglia, A. Vescovi, BMHP1-derived self-assembling peptides: hierarchically assembled structures with self-healing propensity and potential for tissue engineering applications, ACS Nano 5 (3) (2011) 1845–1859.
[39] G. Cerullo, C. Manzoni, L. Luer, D. Polli, Time-resolved methods in biophysics. 4. Broadband pump-probe spectroscopy system with sub-20 fs temporal resolution for the study of energy transfer processes in photosynthesis, Photochemical & Photobiological Sciences: Official Journal of the European Photochemistry Association and the European Society for Photobiology 6 (2) (2007) 135–144.
[40] J.J. Snellenburg, S. Laptenok, R. Seger, K.M. Mullen, I.H.M. van Stokkum, Glotaran: a Java-based graphical user interface for the R package TIMP, J. Stat. Softw. 49 (3) (2012) 1–22.
[41] J. Kisiday, M. Jin, B. Kurz, H. Hung, C. Semino, S. Zhang, A.J. Grodzinsky, Self-assembling peptide hydrogel fosters chondrocyte extracellular matrix production and cell division: implications for cartilage tissue repair, Proc. Natl. Acad. Sci. U. S. A. 99 (15) (2002) 9996–10001.
[42] D. Cigognini, D. Silva, S. Paloppi, F. Gelain, Evaluation of mechanical properties and therapeutic effect of injectable self-assembling hydrogels for spinal cord injury, J. Biomed. Nanotechnol. 10 (2) (2014) 309–323.
[43] J.K. Tripathi, S. Pal, B. Awasthi, A. Kumar, A. Tandon, K. Mitra, N. Chattopadhyay, J.K. Ghosh, Variants of self-assembling peptide, KLD-12 that show both rapid fracture healing and antimicrobial properties, Biomaterials 56 (2015) 92–103.
[44] F. Gelain, D. Cigognini, A. Caprini, D. Silva, B. Colleoni, M. Donega, S. Antonini, B.E. Cohen, A. Vescovi, New bioactive motifs and their use in functionalized self-assembling peptides for NSC differentiation and neural tissue engineering, Nanoscale 4 (9) (2012) 2946–2957.
[45] A. Caprini, D. Silva, I. Zanoni, C. Cunha, C. Volonte, A. Vescovi, F. Gelain, A novel bioactive peptide: assessing its activity over murine neural stem cells and its potential for neural tissue engineering, New Biotechnol. 30 (5) (2013) 552–562.
[46] A. Marchini, A. Raspa, R. Pugliese, M.A. El Malek, V. Pastori, M. Lecchi, A.L. Vescovi, F. Gelain, Multifunctionalized hydrogels foster hNSC maturation in 3D cultures and neural regeneration in spinal cord injuries, Proc. Natl. Acad. Sci. U. S. A. 116 (2019) 7483–7492.
[47] A. Marchini, C. Favoino, F. Gelain, Multi-functionalized self-assembling peptides as reproducible 3D cell culture systems enabling differentiation and survival of various human neural stem cell lines, Front. Neurosci. 14 (2020) 413.
[48] D. Silva, A. Natalello, B. Sanii, R. Vasita, G. Saracino, R.N. Zuckermann, S.M. Doglia, F. Gelain, Synthesis and characterization of designed BMHP1-derived self-assembling peptides for tissue engineering applications, Nanoscale 5 (2) (2013) 704–718.
[49] G.A. Saracino, F. Gelain, Modelling and analysis of early aggregation events of BMHP1-derived self-assembling peptides, J. Biomol. Struct. Dyn. 32 (5) (2014) 759–775.
[50] G.A.A. Saracino, F. Fontana, S. Jekhmane, J.M. Silva, M. Weingarth, F. Gelain, Elucidating self-assembling peptide aggregation via Morphoscanner: a new tool for protein-peptide structural characterization, Advanced Science 5 (8) (2018), 1800471. .
[51] S. Jekhmane, M. Prachar, R. Pugliese, F. Fontana, J. Medeiros-Silva, F. Gelain, M. Weingarth, Design parameters of tissue-engineering scaffolds at the atomic scale, Angew. Chem. 58 (47) (2019) 16943–16951.
[52] Y. Zhu, Z. Dong, U.C. Wejinya, S. Jin, K. Ye, Determination of mechanical properties of soft tissue scaffolds by atomic force microscopy nanoindentation, J. Biomech. 44 (13) (2011) 2356–2361.
[53] G.A. Saracino, D. Cigognini, D. Silva, A. Caprini, F. Gelain, Nanomaterials design and tests for neural tissue engineering, Chem. Soc. Rev. 42 (1) (2013) 225–262.
[54] N.A. Hammond, R.D. Kamm, Mechanical characterization of self-assembling peptide hydrogels by microindentation, J Biomed Mater Res B Appl Biomater 101 (6) (2013) 981–990.
[55] C. Cunha, S. Panseri, O. Villa, D. Silva, F. Gelain, 3D culture of adult mouse neural stem cells within functionalized self-assembling peptide scaffolds, Int. J. Nanomedicine 6 (2011) 943–955.
[56] J.M. Barnes, L. Przybyla, V.M. Weaver, Tissue mechanics regulate brain development, homeostasis and disease, J. Cell Sci. 130 (1) (2017) 71–82.
[57] D. Wirthl, R. Pichler, M. Drack, G. Kettlguber, R. Moser, R. Gerstmayr, F. Hartmann, E. Bradt, R. Kaltseis, C.M. Siket, S.E. Schausberger, S. Hild, S. Bauer, M. Kaltenbrunner, Instant tough bonding of hydrogels for soft machines and electronics, Sci. Adv. 3 (6) (2017), e1700053. .
[58] H. Yuk, B. Lu, X. Zhao, Hydrogel bioelectronics, Chem. Soc. Rev. 48 (2018) 1642–1667.
[59] E. Cerf, R. Sarroukh, S. Tamamizu-Kato, L. Breydo, S. Derclaye, Y.F. Dufrene, V. Narayanaswami, E. Goormaghtigh, J.M. Ruysschaert, V. Raussens, Antiparallel beta-sheet: a signature structure of the oligomeric amyloid beta-peptide, The Biochemical Journal 421 (3) (2009) 415–423.
[60] R. Sarroukh, E. Goormaghtigh, J.M. Ruysschaert, V. Raussens, ATR-FTIR: a "rejuvenated" tool to investigate amyloid proteins, Biochim. Biophys. Acta 1828 (10) (2013) 2328–2338.
[61] T. Sun, H. Han, G.A. Hudalla, Y. Wen, R.R. Pompano, J.H. Collier, Thermal stability of self-assembled peptide vaccine materials, Acta Biomater. 30 (2016) 62–71.
[62] Y. Pan, L. Liu, Y. Zhang, L. Song, Y. Hu, S. Jiang, H. Zhao, Effect of genipin crosslinked layer-by-layer self-assembled coating on the thermal stability, flammability and wash durability of cotton fabric, Carbohydr. Polym. 206 (2019) 396–402.
[63] Nadezda Lapshina, Jonathan Jeffet, Gil Rosenman, Yuval Ebenstein, T. Ellenbogen, Single fluorescent peptide nanodots, ACS Photonics 6 (6) (2019) 1626–1631.
[64] Y. Yu, S. Gim, D. Kim, Z.A. Arnon, E. Gazit, P.H. Seeberger, M. Delbianco, Oligosaccharides self-assemble and show intrinsic optical properties, J. Am. Chem. Soc. 141 (12) (2019) 4833–4838.
[65] F.T. Chan, G.S. Kaminski Schierle, J.R. Kumita, C.W. Bertoncini, C.M. Dobson, C.F. Kaminski, Protein amyloids develop an intrinsic fluorescence signature during aggregation, Analyst 138 (7) (2013) 2156–2162.
[66] D. Pinotsi, L. Grisanti, P. Mahou, R. Gebauer, C.F. Kaminski, A. Hassanali, G.S. Kaminski Schierle, Proton transfer and structure-specific fluorescence in hydrogen bond-rich protein structures, J. Am. Chem. Soc. 138 (9) (2016) 3046–3057.
[67] Fwu-Long Mi, Shin-Shing Shyu, C.-K. Peng, Characterization of ring-opening polymerization of genipin and pH-dependent cross-linking reactions between chitosan and genipin, Journal of Polymer Science Part A 43 (2005) 1985–2000.
[68] R.A. Marcus, Relation between charge transfer absorption and fluorescence spectra and the inverted region, J. Phys. Chem. 93 (8) (1989) 3078–3086.
[69] X. Peng, F. Song, E. Lu, Y. Wang, W. Zhou, J. Fan, Y. Gao, Heptamethine cyanine dyes with a large stokes shift and strong fluorescence: a paradigm for excited-state intramolecular charge transfer, J. Am. Chem. Soc. 127 (12) (2005) 4170–4171.
[70] Dennis H. Oh, Mitsuru Sano, S.G. Boxer, Electroabsorption (Stark effect) spectroscopy of mono- and biruthenium charge-transfer complexes: measurements of changes in dipole moments and other electrooptic properties, J. Am. Chem. Soc. 113 (18) (1991) 6880–6890.
[71] Y. Ishino, K. Miyata, T. Sugimoto, K. Watanabe, Y. Matsumoto, T. Uemura, J. Takeya, Ultrafast exciton dynamics in dinaphtho[2,3-b:2′3′-f]thieno[3,2-b]-thiophene thin films, Physical Chemistry Chemical Physics: PCCP 16 (16) (2014) 7501–7512.
[72] J. Cabanillas-Gonzalez, T. Virgili, A. Gambetta, G. Lanzani, T.D. Anthopoulos, D.M. de Leeuw, Photoinduced transient stark spectroscopy in organic semiconductors: a method for charge mobility determination in the picosecond regime, Phys. Rev. Lett. 96 (10) (2006), 106601. .
[73] M. Segal, M.A. Baldo, R.J. Holmes, S.R. Forrest, Z.G. Soos, Excitonic singlet-triplet ratios in molecular and polymeric organic materials, Phys. Rev. B 68 (2003).
[74] Roland Schmechel, H.v. Seggern, Electronic traps in organic transport layers, Phys. Status Solidi A 201 (6) (2004) 1215–1235.
[75] K. Tao, Z. Fan, L. Sun, P. Makam, Z. Tian, M. Ruegsegger, S. Shaham-Niv, D. Hansford, R. Aizen, Z. Pan, S. Galster, J. Ma, F. Yuan, M. Si, S. Qu, M. Zhang, E. Gazit, J. Li, Quantum confined peptide assemblies with tunable visible to near-infrared spectral range, Nat. Commun. 9 (1) (2018) 3217.
[76] R.A. Mansbach, A.L. Ferguson, Patchy particle model of the hierarchical self-assembly of pi-conjugated optoelectronic peptides, J. Phys. Chem. B 122 (44) (2018) 10219–10236.
[77] K. Tao, W. Hu, B. Xue, D. Chovan, N. Brown, L.J.W. Shimon, O. Maraba, Y. Cao, S.A.M. Tofail, D. Thompson, J. Li, R. Yang, E. Gazit, Bioinspired stable and photoluminescent assemblies for power generation, Adv. Mater. 31 (12) (2019), e1807481.